THE JOURNAL OF PHYSICAL CHEMISTRY B

Article

pubs.acs.org/JPCB

Resonantly Enhanced Nonlinear Optical Probes of Oxidized Multiwalled Carbon Nanotubes at Supported Lipid Bilayers

Alicia C. McGeachy,[†] Laura L. Olenick,[†] Julianne M. Troiano,[†] Ronald S. Lankone,[‡] Eric S. Melby,[§] Thomas R. Kuech,[§] Eseohi Ehimiaghe,[†,#] D. Howard Fairbrother,[‡] Joel A. Pedersen,[§,∥] and Franz M. Geiger*[,†]

[†]Department of Chemistry, Northwestern University, Evanston, Illinois 60208, United States

[‡]Department of Chemistry, Johns Hopkins University, Baltimore, Maryland 21218, United States

[§]Environmental Chemistry and Technology Program, University of Wisconsin, Madison, Wisconsin 53706, United States

[∥]Department of Chemistry, University of Wisconsin, Madison, Wisconsin 53706, United States

Supporting Information

ABSTRACT: With production of carbon nanotubes surpassing billions of tons per annum, concern about their potential interactions with biological systems is growing. Herein, we utilize second harmonic generation spectroscopy, sum frequency generation spectroscopy, and quartz crystal microbalance with dissipation monitoring to probe the interactions between oxidized multiwalled carbon nanotubes (O-MWCNTs) and supported lipid bilayers composed of phospholipids with phosphatidylcholine head groups as the dominant component. We quantify O-MWCNT attachment to supported lipid bilayers under biogeochemically relevant conditions and discern that the interactions occur without disrupting the structural integrity of the lipid bilayers for the systems probed. The extent of O-MWCNT sorption was far below a monolayer even at 100 mM NaCl and was independent of the chemical composition of the supported lipid bilayer.

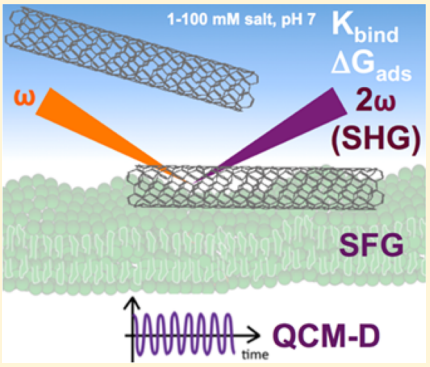

I. INTRODUCTION

Carbon nanotubes (CNTs) have actual and proposed applications in consumer product areas including optics,[1,2] electronics,[3,4] biomedicine,[5] drug delivery,[6−9] environmental remediation,[10−14] and energy technologies.[15,16] Applications and technologies that do not require specific chirality, diameters, or bandgaps often favor multiwalled CNTs (MWCNTs) over single walled carbon nanotubes because of the much lower cost and relative ease of production of MWCNTs.[17] The projected increase in the use of CNT-based nanomaterials, however, raises concern about the potential adverse impacts new technologies utilizing these materials may have on the environment.[18−26] Consequently, the possibility of the environmental release of engineered nanomaterials in general,[19,27] and MWCNTs in particular, and their subsequent interaction with biological systems has motivated laboratory studies of how they interact with biologically relevant systems of varying complexity,[26,28,29] including idealized model systems consisting of phospholipid membranes.[23,30−35] Several studies have indicated that CNTs may penetrate biological membranes, traverse the cell membrane, or lead to alterations in cellular function, including death.[36−43]

In the environment, CNT surfaces are likely to be decorated with oxygen-containing functional groups.[44,45] Oxidized MWCNTs (O-MWCNTs) may thus represent a more realistic model system for studying the biogeochemical consequences of CNT release into the environment than pristine (unoxidized) CNTs.[46,47] Oxygen-containing functional groups are grafted either deliberately into the CNT sidewalls during covalent functionalization strategies or inadvertently as a result of exposure to oxidizing conditions.[48−50] The presence of oxygen-containing functional groups on CNTs increases their hydrophilicity[51,52] and stability in aqueous solutions.[44,53−55] Although concentrations of O-MWCNTs in the environment have yet to be determined, current estimates based on a number of parameters including production rates suggest that CNT concentrations may be as high as several μg/kg of soil.[56] On the other hand, field experiments with natural benthic communities show that 2 mg of MWCNTs/kg aquatic sediment induced detectable changes in the structure of benthic organism communities.[57]

Given the difficulty in determining the concentration of CNTs in environmental settings and the uncertainty associated with current estimates, determining reasonable O-MWCNT concentrations that are also environmentally relevant for experimental laboratory models, is challenging. Electrophysiological measurements conducted by Corredor et al. on suspended planar lipid bilayer membranes composed of 1,2-dioleoyl-*sn*-3-phosphotidylcholine (DOPC) suggest that O-MWCNTs at concentrations as low as 1.6 mg/L can induce

Received: October 7, 2016
Revised: January 12, 2017
Published: January 13, 2017

DOI: 10.1021/acs.jpcb.6b10141
J. Phys. Chem. B 2017, 121, 1321−1329

transmembrane current fluxes and possibly traverse the lipid bilayer.[30] Yi and Chen explored the interactions between O-MWCNTs and DOPC under varying ionic strength and pH conditions using quartz crystal microbalance with dissipation monitoring (QCM-D). They reported no attachment of O-MWCNTs with surface oxygen concentrations of ca. 10% O to DOPC at 100 mM NaCl at pH 7.4 (10 mM HEPES) at O-MWCNT concentrations of 500 μg/L as detected by QCM-D.[33] Though significant progress has been made in exploring the impact of CNTs on biological systems, molecular-level insight into the interactions that occur between O-MWCNTs and biological systems remains limited.

Here, we apply a multipronged approach to investigate the interactions of O-MWCNTs in the ng/L to mg/L concentration range with supported lipid bilayers (SLBs), which have been used as model systems for probing the interaction of O-MWCNT with cellular membranes.[30,34,58,59] We employ, for the first time, second harmonic generation (SHG) to track the adsorption of nanotubes to the SLB and estimate binding equilibria and adsorption free energies. We also report the first vibrational sum frequency generation (SFG) spectra of the carbon tail and headgroups within the lipids comprising the bilayer before, during, and after interaction with O-MWCNTs. Finally, we complement our spectroscopic measurements with mass measurements using QCM-D to estimate the total mass attached. Our use of SLBs most likely prevents us from addressing possible experimental outcomes such as membrane piercing, and the formation of transmembrane channels, which molecular dynamics simulations[34,58,59] and experiments[30,37] indicate can occur under certain conditions. Instead, we focus on the initial step of attachment to the surface. We estimate the interaction free energies and assess whether changes occur to the SLB structure before, during, and after interaction with the O-MWCNTs. Our results in the sub-ppb regime extend current molecular insights toward lower O-MWCNT concentrations than what had been available thus far, which may be of further relevance to biogeochemical conditions.

II. EXPERIMENTAL SECTION

SHG and SFG spectroscopies are surface-general, label-free, and interface-specific techniques that allow interfacial processes to be monitored without the overwhelming contribution from bulk processes. When working with systems as complex as the nano/bio interface, we find that combining several techniques is advantageous in terms of facilitating data interpretation. Therefore, this work combines SHG and SFG spectroscopies, described below in sections II.A–II.E, and QCM-D measurements, described below in section II.F.

II.A. Laser System. Detailed descriptions of our SHG approach can be found elsewhere.[60−63] In one set of experiments, an optical parametric amplifier (OPA-CF, Spectra-Physics) is tuned to a fundamental wavelength between 570 and 610 nm and a variable density filter is used to attenuate the energy of the 120 fs pulses to 0.40 ± 0.05 μJ/pulse, translating to a pump fluence of approximately 60 mJ/cm^2 to avoid thermal degradation of the sample and/or bilayer, as described in section III. The incident beam is focused to a 30 μm diameter focal spot, at an angle just below the angle of total internal reflection, onto a silica/water interface containing an SLB formed as described below. The reflected fundamental light is selectively filtered out through the use of appropriate optical filters and a monochromator tuned to the SHG wavelength. For reasons described below, a second set of experiments consisted of using the output from a 10 nJ, 120 fs oscillator (Spectra Physics Mai Tai, 82 MHz) operating at 800 nm in lieu of the OPA output. In both sets of experiments, the second harmonic signal was collected using single photon counting methods as described elsewhere.[60−63] As described below, SHG bandwidth studies were conducted to confirm that fluorescence or similar sources of radiation other than SHG did not contribute to the observed SHG signal.

II.B. Flow Cell, Substrate, Solution, and Bilayer Preparation. The flow cell and bilayer preparation procedures used in our experiments have been described in detail before.[63] We note that concerns about the potential "stickiness" or adhesion of O-MWCNTs to the PTFE tubing we use in our flow cell prompted us to increase the frequency with which we exchanged our tubing to once every other experiment. Before use, and between trials, the tubing was thoroughly rinsed with methanol, ultrapure water (≥18 MΩ·cm), and buffer solution. All other procedures used to prepare buffers and lipid bilayers were identical to those described earlier.[63] All buffers contained 10 mM Tris adjusted to pH 7.4 using dilute HCl or NaOH as needed and are henceforth referred to as Tris buffer.

For most of the work described herein, we studied SLBs formed from 1,2-dimyristoyl-3-*sn*-glycerophosphatidylcholine (DMPC), as phospholipids bearing a zwitterionic PC headgroup are the majority lipids in the extracellular leaflet of eukaryotic cell membranes.[63] To prepare vesicle suspensions, 2 mg of 1,2-dimyristoyl-*sn*-glycero-3-phosphocholine (DMPC, Avanti Polar Lipids) in chloroform were dried under a gentle stream of N_2. The dried lipids were then placed in a vacuum desiccator overnight to remove any remaining organic solvent, and then stored in the freezer under nitrogen. Prior to use, the dried lipid vesicle films were rehydrated with a 100 mM NaCl, 10 mM Tris, 5 mM $CaCl_2$ solution at pH 7.4 and gently warmed to a temperature above the chain melting temperature (T_m = 24 °C)[64] for approximately 1 h. Vortexing the solution produced a suspension of multilamellar lipid vesicles that was then mechanically extruded through a polycarbonate membrane with a pore size of 0.05 μm (Avanti Polar Lipids). The suspension was passed through the polycarbonate membrane 11 times, as suggested by the manufacturer. Bilayers composed of 1,2-dioleoyl-*sn*-glycero-3-phosphocholine (DOPC) and 1,2-dioleoyl-3-trimethylammonium-propane (DOTAP) were prepared in a similar fashion. The vesicle suspensions were stored in glass scintillation vials or polypropylene Falcon tubes until use. Vesicle-containing suspensions were used within 2 d of preparation. The vesicle fusion method was employed to form supported lipid bilayers.[65] In SHG and SFG experiments, the flow cell was first equilibrated with Tris buffer containing 100 mM NaCl. After acquiring a steady background signal, 4 mL of a 0.5 mg/mL vesicle-containing solution (100 mM NaCl, 10 mM Tris, 5 mM $CaCl_2$, pH 7.4) was introduced into the flow cell. After allowing the SLB to form at the silica/water interface over the course of at least 20 min, the SLB was rinsed with $CaCl_2$-free Tris buffer (100 mM NaCl) to remove remaining intact vesicles.

II.C. Preparation and Characterization of O-MWCNT Suspensions. A detailed procedure for the oxidation of MWCNTs is documented elsewhere.[52,46] Briefly, pristine multiwall carbon nanotubes (MWCNTs) were purchased from NanoLab Inc. (Waltham, MA). The as-received MWCNTs were characterized by the manufacturer to have an outer diameter of 15 ± 5 nm, a length of 5−20 μm, and a carbon purity of >95%. As described in detail in the Supporting

DOI: 10.1021/acs.jpcb.6b10141
J. Phys. Chem. B 2017, 121, 1321−1329

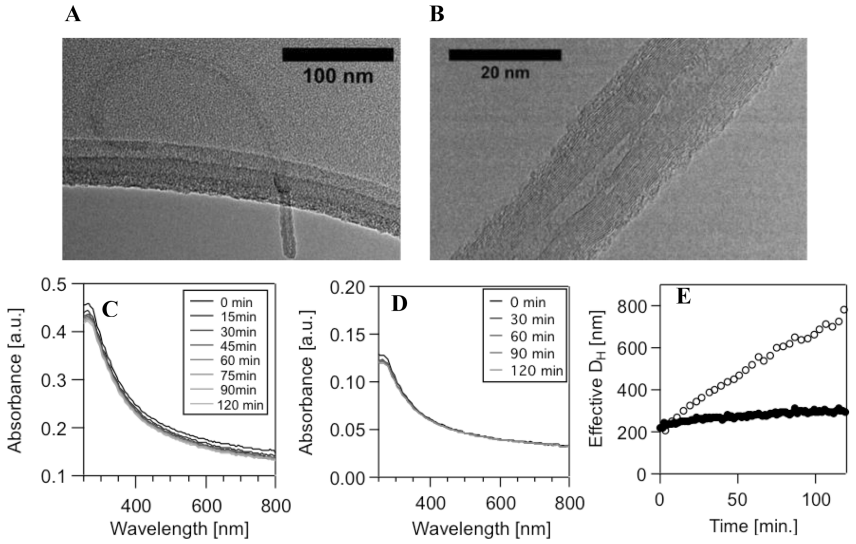

Figure 1. (A) Low- and (B) high-magnification TEM images of O-MWCNTs prepared by refluxing in 70% HNO_3. (C, D) UV−vis absorbance spectra of 1 mg/L (C) O-MWCNT (7% O) and (D) O-MWCNT (12% O) in 100 mM NaCl, 10 mM Tris buffer, pH 7.4, over the span of 2 h. (E) Effective hydrodynamic diameter (D_H) of O-MWCNT with surface oxygen concentrations of 7% O (filled black circles) and 12% O (open circles) MWCNT suspensions at 1 mg/L, 100 mM NaCl, 10 mM Tris buffer, pH 7.4, as a function of time.

Information, we used two different batches of oxidized MWCNTs that we prepared to contain 12 and 7% surface oxygen, denoted below as 7 and 12% O-MWCNTs, using H_2SO_4/HNO_3. Uncertainties are in the 1% range. The CNT purification procedure developed by Bitter et al. (2014)[46] was followed for all O-MWCNTs produced. Transmission electron microscopy (TEM, Philips CM 300) was used to examine the structure of the O-MWCNTs following the oxidation procedure. TEM samples were prepared by dipping a lacey-carbon grid into a colloidal suspension of O-MWCNTs in water; the sample was imaged at 300 kV, and the images were collected with a CCD camera (Figure 1A,B). Figure 1A shows that the oxidation process leaves the MWCNTs structurally intact with approximately 10 walls and lengths on the order of several hundreds of nanometers. Dynamic light scattering (DLS) and laser Doppler microelectrophoresis (Zetasizer Nano ZS, Malvern Instruments, 632.8 nm, 173° backscattering angle) were used to estimate changes in hydrodynamic diameter over time and to measure electrophoretic mobility (EPM) for assessing the stability of aqueous O-MWCNT-containing suspensions used in the SHG, SFG, and QCM-D experiments.

II.D. SHG Experiments. In SHG adsorption experiments, the O-MWCNT-containing suspensions were introduced into the cell at a given nanotube concentration using a flow rate of 2.5 mL/min for a total volume of approximately 8 mL. To avoid changes in SHG signal that could be attributable to changes in ionic strength or pH, the O-MWCNT solutions were prepared such that the conditions of the background electrolyte and pH remained constant (1 or 100 mM NaCl, 10 mM Tris, pH 7.4). The pH of the particle suspensions was determined prior to each introduction and adjusted to pH 7.4 using dilute HCl and NaOH as necessary. Each suspension was vortexed for approximately 20 s immediately prior to introduction into the flow cell.

II.E. SFG Experiments. Following our previously described approach,[61,66] we tune the broadband IR output of an OPA to the C−H stretching region between 2800 and 3000 cm^{-1}. SFG spectra are collected using near total internal reflection geometry and the *ssp* polarization combination, which probes components of the vibrational modes that are oriented perpendicular to the surface. Each SFG spectrum is composed of an average of five acquisitions each integrated over 4 min. In SFG experiments, the SLBs were rinsed with 30 mL of Tris buffer at a flow rate of 1.5 mL/min because of the larger volume of the flow cell used in those experiments. SFG spectra of the SLBs before exposure to O-MWCNTs (Figure 2) agree well with our previous report,[63] and are consistent with the presence of well-formed bilayers.

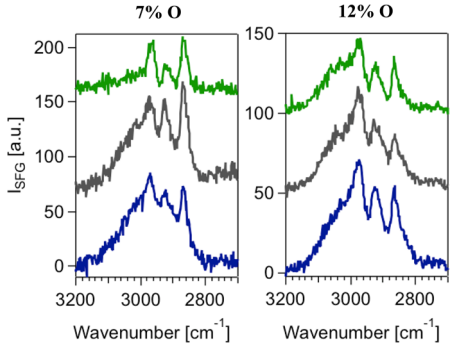

Figure 2. *ssp*-Polarized SFG spectra of SLBs formed from DMPC before (green) and after interaction with 1 mg/L O-MWCNT (gray), and after rinsing with 100 mM NaCl buffer solution (blue) at 100 mM NaCl.

II.F. QCM-D Experiments. QCM-D experiments were conducted using a modified version of our previously described procedures.[63] In these experiments, the particle attachment period was extended to 140 min, and the flow rate was reduced to 10 μL/min. More details are provided in the Supporting Information.

III. RESULTS AND DISCUSSION

III.A. Assessing the Stability of O-MWCNT Suspensions. Our DLS data indicates that some O-MWCNT aggregation occurs over the course of the SHG and SFG experiments, while UV−vis data indicates the absence of

DOI: 10.1021/acs.jpcb.6b10141
J. Phys. Chem. B 2017, 121, 1321−1329

settleable aggregates (Figure 1C,D). Specifically, the UV−vis data shown in Figure 1 indicates that the 7% O and 12% O MWCNTs are stable toward sedimentation over the time scale of the SHG and SFG experiments. Although DLS measurements (Figure 1E) indicate some aggregation of the O-MWCNTs occurs over the time period of the optical experiments (2 h), the increase in the hydrodynamic diameter (D_H) of the 7% O-MWCNTs and 12% O-MWCNTs stabilizes after approximately 20 min at which point our SHG measurements were conducted. Comparable EPM values ($-6.1\ (\pm 2.9) \times 10^{-9}$and $-5.7\ (\pm 1.1) \times 10^{-9}$ $m^2 \cdot V^{-1} \cdot s^{-1}$ for O-MWCNTs with surface oxygen concentrations of 7% and 12% O, respectively) were obtained despite the difference in the relative percentage of oxygen-containing functional groups. The lack of correlation between the atomic percent surface oxygen concentration and the measured electrophoretic mobilities at pH values higher than 6 has been observed in other studies of O-MWCNTs.[54] These various particle stability measurements indicated that the SHG and SFG data are best described as representing the interactions of individual O-MWCNTs and small O-MWCNT aggregates with SLBs.

III.B. Attachment of O-MWCNTs to Supported Lipid Bilayers Prepared from DMPC. We recently determined that, after accounting for the interfacial potential contributed by the SiO_2 substrate, SLBs rich in phospholipids with PC headgroups carry a negative interfacial potential at 100 mM NaCl at pH 7.4,[63] which is important, given the negative surface potentials of the O-MWCNTs used here. Upon exposure to 1 mg/L O-MWCNTs in the presence of 100 mM NaCl buffer, we observe a ca. 200 cm^{-1} broad contribution underneath the relatively sharp vibrational features observed prior to O-MWCNT exposure for 7% O-MWCNTs (Figure 2A) and 12% O-MWCNTs (Figure 2B). We putatively attribute this broad spectral feature to the production of a nonresonant SFG response from the pool of polarizable free electrons associated with the π-electron system of the O-MWCNTs, reminiscent of the well-known nonresonant SFG response from polarizable metals.[67] Upon rinsing the bilayer with O-MWCNT-free solution, the SHG signal remains unchanged, indicating irreversible adsorption of O-MWCNTs to the SLBs over the time scale investigated.

The appearance of a nonresonant response, on top of which ride well-resolved vibrational features of the SLB, is observed in the majority of the experiments conducted across three O-MWCNT samples. However, we note that a subset of experiments conducted with 7% O-MWCNTs produced no change in the SFG signal (i.e., no increased nonresonant background develops; see Supporting Information Figure S7), which we attribute to possible variation in aggregation state or solution stability for the batch used in those specific experiments, though these differences were not evident in UV−vis and DLS measurements.

QCM-D studies conducted under conditions similar to those discussed in the SFG experiments (100 mM NaCl buffer and 1 mg/L 7% O-MWCNTs) reveal a small but measurable frequency shift, $\Delta f = -0.57 \pm 0.16$ Hz (Figure S5). Upon rinsing the SLB formed from DMPC with buffer solution (i.e., no O-MWCNT present), the frequency shift increases to -0.33 ± 0.10 Hz (Figure 3). This observation is attributable to the removal of weakly bound carbon nanotubes, some portion of the bilayer, or both, along with loss of associated water and electrolyte. However, given that the SFG results do not indicate further bilayer alteration (Figure 2), the rinsing likely leads to

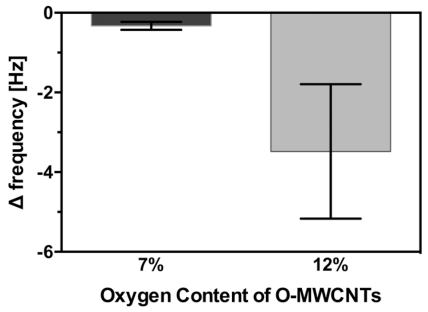

Figure 3. Attachment of O-MWCNTs (1 mg/L) to supported lipid bilayers formed from DMPC at 100 mM NaCl (10 mM Tris buffer, pH 7.4) as determined by QCM-D. Decreases in frequency correspond to increases in mass. Frequency data are reported for the fifth harmonic. Error bars represent one standard deviation (n = 3). Full QCM-D traces are provided in the Supporting Information.

the loss of weakly bound 7% O-MWCNTs. QCM-D studies conducted under the same conditions with 12% O-MWCNTs yield larger frequency shifts of -3.5 ± 1.7 Hz, albeit with larger uncertainties of the point estimate (Figure 3) and no reversibility. The energy dissipation relative to the frequency changes for these systems $(\Delta D_5/(\Delta f_5/5)) = 9.4\ (\pm 2.7) \times 10^{-7}$ and $8.3\ (\pm 2.0) \times 10^{-7}$ Hz^{-1} for the 7 and 12% O-MWCNTs, respectively) precludes application of the Sauerbrey equation to estimate the mass of O-MWCNTs on the SLBs.[68] Nevertheless, the small frequency shifts observed indicate that the surface coverages here are far below a monolayer.

III.C. SHG Control Studies. Given that these experiments are the first to employ SHG to probe O-MWCNTs at liquid/solid interfaces, we briefly discuss outcomes from the control experiments we carried out to assess the validity and origin of the detected nonlinear optical signals. When compared to the bare SLB response at 100 mM NaCl and 10 mM Tris buffer (no O-MWCNTs present), we observed fractional SHG signal intensity increases as large as approximately 20% at λ_{SHG} = 300 nm (kHz amplifier laser source) for all of the O-MWCNTs studied. Adsorption of O-MWCNTs to bare silica or defects in the SLB structure cannot be ruled out as a potential source for the observed SHG signal increases, given that adsorption isotherms for bare silica yield similar fractional increases in SHG intensity though adsorption to the underlying silica support is unlikely given that micron-scale defects in the SLB structure have not been observed. On the basis of QCM-D frequency shifts (24−26 Hz) and surface coverages ($\sim(3.4$ to $4.1) \times 10^{14}$ cm^{-2}), SFG spectroscopy (well-resolved spectra), AFM, and fluorescence microscopy (diffusion coefficients of ~ 2 $\mu m^2/s$), forming supported lipid bilayers via the vesicle fusion method does result in the formation of fluid nearly complete supported lipid bilayers, as was shown in our previously published work.[63] Given the QCM-D results indicating mass uptake upon introducing O-MWCNTs with surface oxygen concentrations of 7 and 12% to SLBs formed from DMPC, we interpret this SHG response to indicate nanotube attachment to the bilayer. Further, attachment of 7% O-MWCNTs to SLBs formed from DMPC depends on ionic strength with no significant change in SHG signal intensity relative to the initial SLB observed at 1 mM NaCl (Figure S6), indicative of a repulsive electrostatic interaction between the O-MWCNTs and the SLBs. Similar trends in the adsorption of O-MWCNT under conditions of increasing ionic strength were also described in other work investigating the interactions of O-

DOI: 10.1021/acs.jpcb.6b10141
J. Phys. Chem. B 2017, 121, 1321−1329

MWCNT and SLBs formed from DOPC.[33] To be clear, the term attachment here should not be taken to imply that covalent bonds are formed. Instead, the expectation is that the O-MWCNTs are physically adsorbed to the SLBs.

To better understand the origin of our SHG signal gains, a second set of SHG experiments were conducted. At λ_{SHG} = 400 nm (MHz oscillator laser source), we observe no change in SHG signal intensity upon interaction of SLBs formed from DMPC with O-MWCNTs (Figure 4). The finding of significant

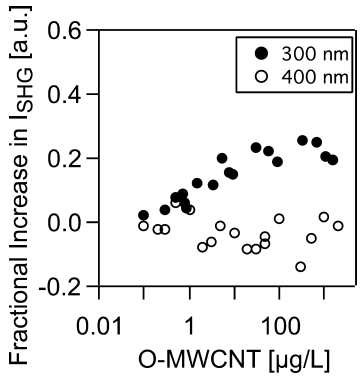

Figure 4. Fractional increase in SHG signal intensity as a function of O-MWCNT concentration, in mg/L, in the presence of supported lipid bilayers formed from DMPC at 100 mM NaCl, 10 mM Tris buffer at pH 7.4 as monitored at 600 nm (λ_{SHG} = 300 nm, filled circles) and 800 nm (λ_{SHG} = 400 nm, open circles) incident wavelengths.

increases in the SHG response at 300 nm that coincides with O-MWCNT addition and a lack of signal increase at 400 nm indicates that SHG resonance enhancement, which can substantially boost signal intensities when the SHG wavelength matches an electronic transition in the surface-bound species,[69−71] may be an important contributor to the SHG signals recorded here. Indeed, given the optical absorbance features of the O-MWCNTs toward the shorter wavelengths (Figure 1), it is likely that our experiments are approaching electronic two-photon resonance with the $\pi \rightarrow \pi^*$ transitions of the nanotubes. However, further experiments using SHG spectroscopy with varying incident and SHG wavelengths are needed to unambiguously assess the role of resonance enhancement here.

To determine the damage threshold of the SLB systems and the bare silica substrate in the presence of 2 mg/L O-MWCNT, we introduced, in two separate experiments, two concentrations (1 and 2 mg/L) of O-MWCNTs in 100 mM NaCl buffer to the flow cell and increased the incident visible pulse energy in increments of 0.05 μJ up to 0.5 μJ. Fits of a power function to the SHG intensity as a function of pulse energy yield a quadratic dependence at a concentration of 1 mg/L (Figure 5A) but deviate somewhat (P = 2.6) at a concentration of 2 mg/L (Figure 5B). Departures from the expected quadratic dependence indicate optical breakdown, optical processes other than SHG, or sample damage, which may be attributable to nanotube aggregation specifically at the interface, as opposed to the bulk aqueous solution, and strong absorbance at this high concentration and pulse energy. Given the data shown in Figure 5A and B, all SHG experiments were carried out using nanotube concentrations ≤1 mg/L and incident pulse energies of 0.40 ± 0.05 μJ so as to remain within the regime of well-behaved SHG responses.

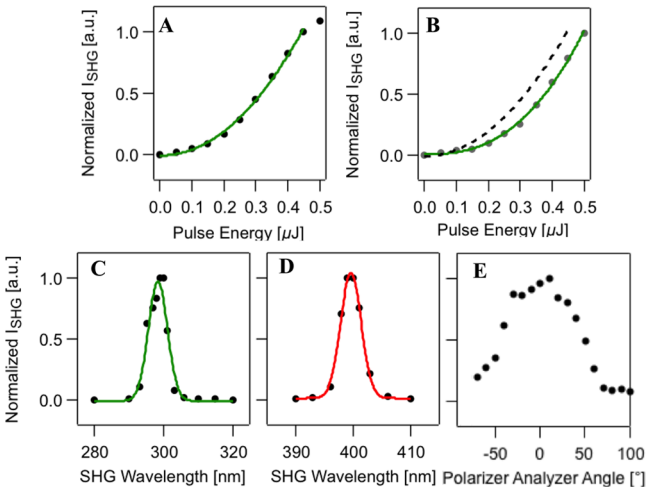

Figure 5. (A) Normalized SHG intensity as a function of pulse energy at 600 nm fundamental light field for 1 mg/L O-MWCNT interacting with an SLB formed from DMPC at 100 mM NaCl. The green curve is a power function of the form $y = A + Bx^p$, where p = 2.1 ± 0.1. (B) Normalized SHG intensity as a function of pulse energy at 600 nm fundamental light field for 2 mg/L O-MWCNT interacting with an SLB formed from DMPC at 100 mM NaCl. The green curve is a power function of the form $y = A + Bx^p$, where p = 2.6 ± 0.1. The black dashed line is a representative quadratic curve with a power of 2. (C) SHG intensity with the fundamental beam at 600 nm collected as a function of monochromator wavelength and Gaussian fit (solid green line) resulting in 3.9 ± 0.4 nm bandwidth for 2 mg/L concentration of O-MWCNT interacting with an SLB formed from DMPC at 100 mM NaCl. (D) SHG intensity with the fundamental beam at 800 nm collected as a function of monochromator wavelength and Gaussian fit (solid red line) resulting in 2.5 ± 0.1 nm bandwidth for 2 mg/L concentration of O-MWCNT interacting with an SLB formed from DMPC at 100 mM NaCl. (E) SHG intensity as a function of output polarization angle aligned with the surface normal while probing with p-polarized fundamental light field for 2 mg/L O-MWCNT interacting with a SLB formed from DMPC at 100 mM NaCl.

Additional SHG bandwidth studies show that SHG signals recorded at λ_{SHG} of 300 and 400 nm (Figure 5C and D, respectively) are well behaved, showing no evidence of fluorescence or radiation other than SHG entering the photomultiplier tube. Finally, SHG polarization studies carried out with p-polarized incident light and at λ_{SHG} = 300 nm show that the SHG signal is well polarized along the surface normal (Figure 5E).

III.D. SHG Adsorption Isotherm Measurements. Having verified that the nonlinear signal response was indeed due to SHG, we proceeded to record the SHG response as a function of O-MWCNT (7% O) concentration. Figure 6 shows the average of 18 individual adsorption isotherm measurements, each time using a newly formed SLB and newly prepared O-MWCNT (7% O) suspension. We find that the SHG response increases with O-MWCNT (7% O) concentration and begins to plateau at approximately 10 μg/L in the case of all O-MWCNTs investigated here, regardless of the surface oxygen concentration. This plateau indicates some limiting surface coverage has been reached.

To provide an estimate for the interaction energy, we fit the Langmuir adsorption model[72−74] to the SHG adsorption isotherms. The Langmuir fit yielded an apparent equilibrium constant, K_L^{app}, of 1.2 ± 0.2 and 2.0 ± 0.4 L/μg for 100 mM NaCl buffer, corresponding to adsorption free energy estimates

DOI: 10.1021/acs.jpcb.6b10141
J. Phys. Chem. B 2017, 121, 1321−1329

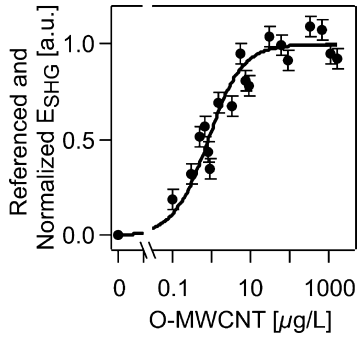

Figure 6. SHG *E*-fields as a function of O-MWCNT concentration (7% O), in μg/L, collected at 300 nm, normalized to maximum *E*-field at high O-MWCNT concentration recorded at 100 mM NaCl, 25 °C, pH 7.4, in the presence of a SLB formed from DMPC at 100 mM NaCl and referenced to the SHG signal from an SLB formed from DMPC at the silica/water interface (filled circles). The black solid line is a fit of the Langmuir adsorption model to the experimental data collected at 100 mM NaCl in the presence of a SLB formed from DMPC, specifically of the form $\theta = K_L^{app}C/(1 + K_L^{app}C)$, where K_L^{app} is the apparent equilibrium attachment constant, C is the concentration of O-MWCNT in μg/L, and θ is the relative SHG *E*-field. Error bars are generated from the standard deviation of data points collected at high particle concentration.

of −52 ± 0.4 and −53 ± 0.8 kJ/mol$_C$ for the O-MWCNTs with surface oxygen concentrations of 7 and 12%, respectively. In this analysis, we used the 55.5 M (or 10^9 μg/L) concentration of water as a standard state for adsorption from solution.[75] Departures from the Langmuir model could be attributable to the lack of reversibility, (direct or indirect) particle−particle interactions (e.g., O-MWCNT aggregation), and the heterogeneous nature of O-MWCNTs, and are likely to be masked by the uncertainty in the reported point estimate.

III.E. O-MWCNT Adsorption to SLBs Prepared from DOPC and DOPC/DOTAP. O-MWCNTs with surface oxygen concentrations of 8% O also adsorbed to SLBs composed of zwitterionic DOPC and DOPC bilayers containing cationic 1,2-dioleoyl-3-trimethylammoniumpropane (DOTAP) (Figure 7). (The batch of O-MWCNTs used in these experiments had a surface oxygen concentration of 8%, while those described in the previous sections had 7% O.) While we hypothesized that the adsorption of these negatively charged O-MWCNT particles would be higher in the presence of DOTAP, a cationic lipid, our SHG signals were comparable across SLBs formed from DOPC, DMPC, and 9:1 DOPC/DOTAP (Figure 7). Given that the surface charges of the pure SLB formed from DOPC and 9:1 DOPC/DOTAP are comparable,[63] the lack of a significant difference in the adsorption behavior for these two bilayer systems is not surprising.

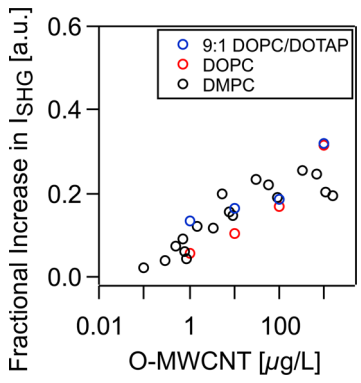

Figure 7. Fractional increase in SHG signal intensity as a function of O-MWCNT concentration, in μg/L, in the presence of supported lipid bilayers formed from 9:1 DOPC/DOTAP (blue open circles), DOPC (red open circles), and DMPC (black open circles) at 100 mM NaCl, 10 mM Tris buffer at pH 7.4. For both the DOPC and 9:1 DOPC/DOTAP SLBs, the O-MWCNTs used have surface oxygen concentrations of 8%, while, for the interaction studies involving DMPC, the concentration is 7% O.

IV. POSSIBLE INTERACTION MECHANISM AND CONCLUSIONS

The results from our SHG, SFG, and QCM-D studies show that O-MWCNTs attach to the SLBs probed here at 100 mM NaCl to a small extent. Adsorption of the CNTs to the SLBs likely does not cause significant disruption or displacement of the SLB, as indicated by the retention of the characteristic SFG spectral features associated with DMPC, despite the development of a strong nonresonant background. Yi and Chen[33] previously reported no attachment of O-MWCNTs (10.6% oxygen) to SLBs composed of DOPC below a NaCl concentration of 200 mM at pH 7.3 (0.2 mM $NaHCO_3$) at 37 °C. The two studies differed with respect to lipids used to form SLBs (DOPC vs DMPC), O-MWCNT concentration, the nature and concentration of the buffer, flow rate, and, likely most importantly, temperature. Nonetheless, similar to the results of Yi and Chen,[33] we observe more attachment to SLBs formed from DMPC or DOPC at higher ionic strength and no attachment at lower ionic strength (1 mM NaCl).

As the O-MWCNTs carry small negative zeta potentials under the conditions of the experiments[33,54,55] and given that SLBs composed of lipids having zwitterionic headgroups carry negative interfacial potentials,[56] the mechanism by which O-MWCNTs adsorb to SLBs formed from DMPC and DOPC likely involves sizable entropy gains as water molecules and electrolyte ions are displaced upon attachment of the nanotubes. Coulomb repulsion between the like-charged O-MWCNTs and the SLBs are thus overcome. Indeed, SHG experiments using bilayers prepared from 9:1 mixtures of DOPC/DOTAP, which are also associated with a negative interfacial potential under the experimental conditions,[63] yield comparable fractional increases in SHG intensity upon exposure to O-MWCNTs as that of DOPC and DMPC further supporting our conclusion.

In summary, we have employed SHG and SFG spectroscopy to directly probe O-MWCNTs interacting with supported lipid bilayers. We showed that O-MWCNTs adsorb to SLBs rich in PC lipids at 100 mM NaCl under the conditions explored in this study and at concentrations in the sub-ng/L range. Resonantly enhanced SHG spectroscopy served as a chemically specific probe and is demonstrated to provide higher sensitivity to sub-μg/L O-MWCNT adsorption processes than QCM-D. We also showed that adsorption of O-MWCNTs to SLBs does not result in significant disruption or displacement of the lipid bilayer, as indicated by SFG spectroscopy. We cannot, however, rule out the formation of pores or assess the extent of local disruption to the bilayer.

■ ASSOCIATED CONTENT

Supporting Information

The Supporting Information is available free of charge on the ACS Publications website at DOI: 10.1021/acs.jpcb.6b10141.

DOI: 10.1021/acs.jpcb.6b10141
J. Phys. Chem. B 2017, 121, 1321−1329

Experimental details and control studies; SHG adsorption isotherms with SLBs formed from DOPC and 9:1 DOPC/DOTAP; SHG and SFG adsorption studies with SLBs formed from DMPC (PDF)

AUTHOR INFORMATION

Corresponding Author

*E-mail: geigerf@chem.northwestern.edu.

ORCID

Joel A. Pedersen: 0000-0002-3918-1860

Franz M. Geiger: 0000-0001-8569-4045

Present Address

[#]Feinberg School of Medicine, Northwestern University, Chicago, IL 60611.

Notes

The authors declare no competing financial interest.

ACKNOWLEDGMENTS

This work was supported by the National Science Foundation Center for Chemical Innovation Program, through the Center for Sustainable Nanotechnology under Grant No. CHE-1503408. A.C.M. and J.M.T. gratefully acknowledge support through the NSF Graduate Research Fellowship Program (GRFP). DLS and XPS work was performed in the Keck II facility of NU*ANCE* Center at Northwestern University. The NU*ANCE* Center is supported by NSEC (NSF EEC-0647560), MRSEC (NSF DMR-1121262), the Keck Foundation, the State of Illinois, and Northwestern University. We acknowledge Dr. Ken Livi and Anna Goodridge for TEM imaging.

REFERENCES

(1) Shriyan, S. K.; Fontecchio, A. K. Analysis of Effects of Oxidized Multiwalled Carbon Nanotubes on Electro-Optic Polymer/Liquid Crystal Thin Film Gratings. *Opt. Express* **2010**, *18*, 24842−24852.

(2) Taib, N. A. M.; Bidin, N.; Haris, H.; Adnan, N. N.; Ahmad, M. F. S.; Harun, S. W. Multi-Walled Carbon Nanotubes Saturable Absorber in Q-Switching Flashlamp Pumped Nd:YAG Laser. *Opt. Laser Technol.* **2016**, *79*, 193−197.

(3) Huang, Z. L.; Gao, M.; Yan, Z. C.; Pan, T. S.; Liao, F. Y.; Lin, Y. Flexible Infrared Detectors Based on P-N Junctions of Multi-Walled Carbon Nanotubes. *Nanoscale* **2016**, *8*, 9592−9599.

(4) Wang, D.; Li, H. Y.; Li, M. F.; Jiang, H. Q.; Xia, M.; Zhou, Z. Stretchable Conductive Polyurethane Elastomer in Situ Polymerized with Multi-Walled Carbon Nanotubes. *J. Mater. Chem. C* **2013**, *1*, 2744−2749.

(5) Servant, A.; Jacobs, I.; Bussy, C.; Fabbro, C.; da Ros, T.; Pach, E.; Ballesteros, B.; Prato, M.; Nicolay, K.; Kostarelos, K. Gadolinium-Functionalised Multi-Walled Carbon Nanotubes as a T-1 Contrast Agent for MRI Cell Labelling and Tracking. *Carbon* **2016**, *97*, 126−133.

(6) Fedeli, S.; Brandi, A.; Venturini, L.; Chiarugi, P.; Giannoni, E.; Paoli, P.; Corti, D.; Giambastiani, G.; Tuci, G.; Cicchi, S. The "Click-on-Tube" Approach for the Production of Efficient Drug Carriers Based on Oxidized Multi-Walled Carbon Nanotubes. *J. Mater. Chem. B* **2016**, *4*, 3823−3831.

(7) Mandal, B.; Das, D.; Rameshbabu, A. P.; Dhara, S.; Pal, S. A Biodegradable, Biocompatible Transdermal Device Derived from Carboxymethyl Cellulose and Multi-Walled Carbon Nanotubes for Sustained Release of Diclofenac Sodium. *RSC Adv.* **2016**, *6*, 19605−19611.

(8) Afshari, R.; Mazinani, S.; Abdouss, M. Nanohybrid Nanoparticles Based on Chitosan/Functionalized Carbon Nanotubes as Anti-HIV Nanocarrier. *Nano* **2015**, *10*, 1550010.

(9) Moradian, H.; Fasehee, H.; Keshvari, H.; Faghihi, S. Poly-(Ethyleneimine) Functionalized Carbon Nanotubes as Efficient Nano-Vector for Transfecting Mesenchymal Stem Cells. *Colloids Surf., B* **2014**, *122*, 115−125.

(10) Mubarak, N. M.; Sahu, J. N.; Abdullah, E. C.; Jayakumar, N. S. Removal of Heavy Metals from Wastewater Using Carbon Nanotubes. *Sep. Purif. Rev.* **2014**, *43*, 311−338.

(11) Das, R.; Ali, M. E.; Abd Hamid, S. B.; Ramakrishna, S.; Chowdhury, Z. Z. Carbon Nanotube Membranes for Water Purification: A Bright Future in Water Desalination. *Desalination* **2014**, *336*, 97−109.

(12) Kim, S. H.; Umar, A.; Kumar, R.; Algarni, H.; Al-Assiri, M. S. Poly(Acrylic Acid)/Multi-Walled Carbon Nanotube Composites: Efficient Scaffold for Highly Sensitive 2-Nitrophenol Chemical Sensor. *Nanosci. Nanotechnol. Lett.* **2016**, *8*, 200−206.

(13) Sun, H. Q.; Kwan, C.; Suvorova, A.; Ang, H. M.; Tade, M. O.; Wang, S. B. Catalytic Oxidation of Organic Pollutants on Pristine and Surface Nitrogen-Modified Carbon Nanotubes with Sulfate Radicals. *Appl. Catal., B* **2014**, *154*−*155*, 134−141.

(14) Gu, H. B.; Rapole, S. B.; Huang, Y. D.; Cao, D. M.; Luo, Z. P.; Wei, S. Y.; Guo, Z. H. Synergistic Interactions between Multi-Walled Carbon Nanotubes and Toxic Hexavalent Chromium. *J. Mater. Chem. A* **2013**, *1*, 2011−2021.

(15) Salunkhe, R. R.; Ahn, H.; Kim, J. H.; Yamauchi, Y. Rational Design of Coaxial Structured Carbon Nanotube-Manganese Oxide ($CNT-MnO_2$) for Energy Storage Application. *Nanotechnology* **2015**, *26*, 204004.

(16) De Nicola, F.; Salvato, M.; Cirillo, C.; Crivellari, M.; Boscardin, M.; Scarselli, M.; Nanni, F.; Cacciotti, I.; De Crescenzi, M.; Castrucci, P. Record Efficiency of Air-Stable Multi-Walled Carbon Nanotube/Silicon Solar Cells. *Carbon* **2016**, *101*, 226−234.

(17) De Volder, M. F. L.; Tawfick, S. H.; Baughman, R. H.; Hart, A. J. Carbon Nanotubes: Present and Future Commercial Applications. *Science* **2013**, *339*, 535−539.

(18) Peijnenburg, W. J. G. M.; et al. A Review of the Properties and Processes Determining the Fate of Engineered Nanomaterials in the Aquatic Environment. *Crit. Rev. Environ. Sci. Technol.* **2015**, *45*, 2084−2134.

(19) Nel, A. E.; Madler, L.; Velegol, D.; Xia, T.; Hoek, E. M. V.; Somasundaran, P.; Klaessig, F.; Castranova, V.; Thompson, M. Understanding Biophysicochemical Interactions at the Nano-Bio Interface. *Nat. Mater.* **2009**, *8*, 543−557.

(20) Chen, C.; Li, Y.-F.; Qu, Y.; Chai, Z.; Zhao, Y. Advanced Nuclear Analytical and Related Techniques for the Growing Challenges in Nanotoxicology. *Chem. Soc. Rev.* **2013**, *42*, 8266−8303.

(21) Xiao, Y.; Wiesner, M. R. Characterization of Surface Hydrophobicity of Engineered Nanoparticles. *J. Hazard. Mater.* **2012**, *215*−*216*, 146−151.

(22) Pelaz, B.; Charron, G.; Pfeiffer, C.; Zhao, Y.; de la Fuente, J. M.; Liang, X.-J.; Parak, W. J.; del Pino, P. Interfacing Engineered Nanoparticles with Biological Systems: Anticipating Adverse Nano-Bio Interactions. *Small* **2013**, *9*, 1573−1584.

(23) Chen, K. L.; Bothun, G. D. Nanoparticles Meet Cell Membranes: Probing Nonspecific Interactions. Using Model Membranes. *Environ. Sci. Technol.* **2014**, *48*, 873−880.

(24) Hassellöv, M.; Readman, J.; Ranville, J.; Tiede, K. Nanoparticle Analysis and Characterization Methodologies in Environmental Risk Assessment of Engineered Nanoparticles. *Ecotoxicology* **2008**, *17*, 344−361.

(25) Yi, P.; Chen, K. L. Influence of Solution Chemistry on the Release of Multiwalled Carbon Nanotubes from Silica Surfaces. *Environ. Sci. Technol.* **2013**, *47*, 12211−12218.

(26) Sarma, S. J.; Bhattacharya, I.; Brar, S. K.; Tyagi, R. D.; Surampalli, R. Y. Carbon Nanotube-Bioaccumulation and Recent Advances in Environmental Monitoring. *Crit. Rev. Environ. Sci. Technol.* **2015**, *45*, 905−938.

(27) Murphy, C. J.; et al. Biological Responses to Engineered Nanomaterials: Needs for the Next Decade. *ACS Cent. Sci.* **2015**, *1*, 117−123.

DOI: 10.1021/acs.jpcb.6b10141
J. Phys. Chem. B 2017, 121, 1321−1329

(28) Bussy, C.; Pinault, M.; Cambedouzou, J.; Landry, M. J.; Jegou, P.; Mayne-L'hermite, M.; Launois, P.; Boczkowski, J.; Lanone, S. Critical Role of Surface Chemical Modifications Induced by Length Shortening on Multi-Walled Carbon Nanotubes-Induced Toxicity. *Part. Fibre Toxicol.* **2012**, *9*, 46.
(29) Luan, B. Q.; Huynh, T.; Zhou, R. H. Complete Wetting of Graphene by Biological Lipids. *Nanoscale* **2016**, *8*, 5750−5754.
(30) Corredor, C.; Hou, W.-C.; Klein, S. A.; Moghadam, B. Y.; Goryll, M.; Doudrick, K.; Westerhoff, P.; Posner, J. D. Disruption of Model Cell Membranes by Carbon Nanotubes. *Carbon* **2013**, *60*, 67−75.
(31) Sanchez, V. C.; Jachak, A.; Hurt, R. H.; Kane, A. B. Biological Interactions of Graphene-Family Nanomaterials: An Interdisciplinary Review. *Chem. Res. Toxicol.* **2012**, *25*, 15−34.
(32) Carney, R. P.; Astier, Y.; Carney, T. M.; Voitchovsky, K.; Silva, P. H. J.; Stellacci, F. Electrical Method to Quantify Nanoparticle Interaction with Lipid Bilayers. *ACS Nano* **2013**, *7*, 932−942.
(33) Yi, P.; Chen, K. L. Interaction of Multiwalled Carbon Nanotubes with Supported Lipid Bilayers and Vesicles as Model Biological Membranes. *Environ. Sci. Technol.* **2013**, *47*, 5711−5719.
(34) Gangupomu, V. K.; Capaldi, F. M. Interactions of Carbon Nanotube with Lipid Bilayer Membranes. *J. Nanomater.* **2011**, *2011*, 830436.
(35) Jimenez-Cruz, C. A.; Kang, S. G.; Zhou, R. H. Large Scale Molecular Simulations of Nanotoxicity. *Wiley Interdiscip. Rev.: Syst. Biol. Med.* **2014**, *6*, 329−343.
(36) Saria, R.; Mouchet, F.; Perrault, A.; Flahaut, E.; Laplanche, C.; Boutonnet, J. C.; Pinelli, E.; Gauthier, L. Short Term Exposure to Multi-Walled Carbon Nanotubes Induce Oxidative Stress and DNA Damage in Xenopus Laevis Tadpoles. *Ecotoxicol. Environ. Saf.* **2014**, *107*, 22−29.
(37) Mu, Q. X.; Broughton, D. L.; Yan, B. Endosomal Leakage and Nuclear Translocation of Multiwalled Carbon Nanotubes: Developing a Model for Cell Uptake. *Nano Lett.* **2009**, *9*, 4370−4375.
(38) Bottini, M.; Bruckner, S.; Nika, K.; Bottini, N.; Bellucci, S.; Magrini, A.; Bergamaschi, A.; Mustelin, T. Multi-Walled Carbon Nanotubes Induce T Lymphocyte Apoptosis. *Toxicol. Lett.* **2006**, *160*, 121−126.
(39) Cui, D. X.; Tian, F. R.; Ozkan, C. S.; Wang, M.; Gao, H. J. Effect of Single Wall Carbon Nanotubes on Human HEK 293 Cells. *Toxicol. Lett.* **2005**, *155*, 73−85.
(40) Monteiro-Riviere, N. A.; Nemanich, R. J.; Inman, A. O.; Wang, Y. Y. Y.; Riviere, J. E. Multi-Walled Carbon Nanotube Interactions with Human Epidermal Keratinocytes. *Toxicol. Lett.* **2005**, *155*, 377−384.
(41) Murr, L. E.; Garza, K. M.; Soto, K. F.; Carrasco, A.; Powell, T. G.; Ramirez, D. A.; Guerrero, P. A.; Lopez, D. A.; Venzor, J., 3rd Cytotoxicity Assessment of Some Carbon Nanotubes and Related Carbon Nanoparticle Aggregates and the Implications for Anthropogenic Carbon Nanotube Aggregates in the Environment. *Int. J. Environ. Res. Public Health* **2005**, *2*, 31−42.
(42) Shi, X. H.; Kong, Y.; Gao, H. J. Coarse Grained Molecular Dynamics and Theoretical Studies of Carbon Nanotubes Entering Cell Membrane. *Acta Mech. Sin.* **2008**, *24*, 161−169.
(43) Pogodin, S.; Baulin, V. A. Can a Carbon Nanotube Pierce through a Phospholipid Bilayer? *ACS Nano* **2010**, *4*, 5293−5300.
(44) Bai, Y. C.; Wu, F. C.; Lin, D. H.; Xing, B. S. Aqueous Stabilization of Carbon Nanotubes: Effects of Surface Oxidization and Solution Chemistry. *Environ. Sci. Pollut. Res.* **2014**, *21*, 4358−4365.
(45) Flores-Cervantes, D. X.; Maes, H. M.; Schaffer, A.; Hollender, J.; Kohler, H. P. E. Slow Biotransformation of Carbon Nanotubes by Horseradish Peroxidase. *Environ. Sci. Technol.* **2014**, *48*, 4826−4834.
(46) Bitter, J. L.; Yang, J.; Milani, S. B.; Jafvert, C. T.; Fairbrother, D. H. Transformations of Oxidized Multiwalled Carbon Nanotubes Exposed to UVC (254 nm) Irradiation. *Environ. Sci.: Nano* **2014**, *1*, 324−337.
(47) Yang, J.; Bitter, J. L.; Smith, B. A.; Fairbrother, D. H.; Ball, W. P. Transport of Oxidized Multi-Walled Carbon Nanotubes through Silica Based Porous Media: Influences of Aquatic Chemistry, Surface Chemistry, and Natural Organic Matter. *Environ. Sci. Technol.* **2013**, *47*, 14034−14043.
(48) Savage, T.; et al. Photoinduced Oxidation of Carbon Nanotubes. *J. Phys.: Condens. Matter* **2003**, *15*, 5915−5921.
(49) Rosca, I. D.; Watari, F.; Uo, M.; Akasaka, T. Oxidation of Multiwalled Carbon Nanotubes by Nitric Acid. *Carbon* **2005**, *43*, 3124−3131.
(50) Wang, Y.; Iqbal, Z.; Mitra, S. Rapidly Functionalized, Water-Dispersed Carbon Nanotubes at High Concentration. *J. Am. Chem. Soc.* **2006**, *128*, 95−99.
(51) Yi, P.; Chen, K. L. Influence of Surface Oxidation on the Aggregation and Deposition Kinetics of Multiwalled Carbon Nanotubes in Monovalent and Divalent Electrolytes. *Langmuir* **2011**, *27*, 3588−3599.
(52) Wepasnick, K. A.; Smith, B. A.; Schrote, K. E.; Wilson, H. K.; Diegelmann, S. R.; Fairbrother, D. H. Surface and Structural Characterization of Multi-Walled Carbon Nanotubes Following Different Oxidative Treatments. *Carbon* **2011**, *49*, 24−36.
(53) Zhang, Q.; Huang, J.-Q.; Qian, W.-Z.; Zhang, Y.-Y.; Wei, F. The Road for Nanomaterials Industry: A Review of Carbon Nanotube Production, Post-Treatment, and Bulk Applications for Composites and Energy Storage. *Small* **2013**, *9*, 1237−1265.
(54) Smith, B.; Wepasnick, K.; Schrote, K. E.; Cho, H.-H.; Ball, W. P.; Fairbrother, D. H. Influence of Surface Oxides on the Colloidal Stability of Multi-Walled Carbon Nanotubes: A Structure-Property Relationship. *Langmuir* **2009**, *25*, 9767−9776.
(55) Smith, B.; Wepasnick, K.; Schrote, K. E.; Bertele, A. H.; Ball, W. P.; O'Melia, C.; Fairbrother, D. H. Colloidal Properties of Aqueous Suspensions of Acid-Treated, Multi-Walled Carbon Nanotubes. *Environ. Sci. Technol.* **2009**, *43*, 819−825.
(56) Sun, T. Y.; Bornhoft, N. A.; Hungerbuhler, K.; Nowack, B. Dynamic Probabilistic Modeling of Environmental Emissions of Engineered Nanomaterials. *Environ. Sci. Technol.* **2016**, *50*, 4701−4711.
(57) Velzeboer, I.; Peeters, E.; Koelmans, A. A. Multiwalled Carbon Nanotubes at Environmentally Relevant Concentrations Affect the Composition of Benthic Communities. *Environ. Sci. Technol.* **2013**, *47*, 7475−7482.
(58) Lelimousin, M.; Sansom, M. S. P. Membrane Perturbation by Carbon Nanotube Insertion: Pathways to Internalization. *Small* **2013**, *9*, 3639−3646.
(59) Prylutska, S.; et al. Comparative Study of Membranotropic Action of Single- and Multi-Walled Carbon Nanotubes. *J. Biosci. Bioeng.* **2013**, *115*, 674−679.
(60) Saslow Gomez, S. A.; Jordan, D. S.; Troiano, J. M.; Geiger, F. M. Uranyl Adsorption at the Muscovite (Mica)/Water Interface Studied by Second Harmonic Generation. *Environ. Sci. Technol.* **2012**, *46*, 11154−11161.
(61) Hayes, P. L.; Malin, J. N.; Konek, C. T.; Geiger, F. M. Interaction of Nitrate, Barium, Strontium and Cadmium Ions with Fused Quartz/Water Interfaces Studied by Second Harmonic Generation. *J. Phys. Chem. A* **2008**, *112*, 660−668.
(62) Achtyl, J. L.; Vlassiouk, I. V.; Surwade, S. P.; Fulvio, P. F.; Dai, S.; Geiger, F. M. Interaction of Magnesium Ions with Pristine Single-Layer and Defected Graphene/Water Interfaces Studied by Second Harmonic Generation. *J. Phys. Chem. B* **2014**, *118*, 7739−7749.
(63) Troiano, J. M.; et al. Direct Probes of 4 Nm Diameter Gold Nanoparticles Interacting with Supported Lipid Bilayers. *J. Phys. Chem. C* **2015**, *119*, 534−546.
(64) Marra, J.; Israelachvili, J. Direct Measurements of Forces between Phosphatidylcholine and Phosphatidylethanolamine Bilayers in Aqueous-Electrolyte Solutions. *Biochemistry* **1985**, *24*, 4608−4618.
(65) Anderson, T. H.; Min, Y.; Weirich, K. L.; Zeng, H.; Fygenson, D.; Israelachvili, J. N. Formation of Supported Bilayers on Silica Substrates. *Langmuir* **2009**, *25*, 6997−7005.
(66) Dogangun, M.; Hang, M. N.; Troiano, J. M.; McGeachy, A. C.; Melby, E. S.; Pedersen, J. A.; Hamers, R. J.; Geiger, F. M. Alteration of Membrane Compositional Asymmetry by Licoo2 Nanosheets. *ACS Nano* **2015**, *9*, 8755−8765.

DOI: 10.1021/acs.jpcb.6b10141
J. Phys. Chem. B 2017, 121, 1321−1329

(67) Covert, P. A.; Hore, D. K. Assessing the Gold Standard: The Complex Vibrational Nonlinear Susceptibility of Metals. *J. Phys. Chem. C* **2015**, *119*, 271−276.
(68) Reviakine, I.; Johannsmann, D.; Richter, R. P. Hearing What You Cannot See and Visualizing What You Hear: Interpreting Quartz Crystal Microbalance Data from Solvated Interfaces. *Anal. Chem.* **2011**, *83*, 8838−8848.
(69) Corn, R. M.; Higgins, D. A. Optical Second Harmonic Generation as a Probe of Surface Chemistry. *Chem. Rev.* **1994**, *94*, 107.
(70) Geiger, F. M. Second Harmonic Generation, Sum Frequency Generation, and $\chi^{(3)}$: Dissecting Environmental Interfaces with a Nonlinear Optical Swiss Army Knife. *Annu. Rev. Phys. Chem.* **2009**, *60*, 61−83.
(71) Eisenthal, K. B. Liquid Interfaces Probed by Second-Harmonic and Sum-Frequency Spectroscopy. *Chem. Rev.* **1996**, *96*, 1343−1360.
(72) Langmuir, D. *Aqueous Environmental Chemistry*; Prentice Hall: Upper Saddle River, NJ, 1997.
(73) Masel, R. I. *Principles of Adsorption and Reaction on Solid Surfaces*; John Wiley & Sons: New York, 1996.
(74) Somorjai, G. A. *Chemistry in Two Dimensions*; Cornell University Press: Ithaca, NY, 1981.
(75) Adamson, A. W. *Physical Chemistry of Surfaces*, 5th ed.; John Wiley & Sons: New York, 1990.

DOI: 10.1021/acs.jpcb.6b10141
J. Phys. Chem. B 2017, 121, 1321−1329